LONG-WAVELENGTH 256X256 GaAs/AlGaAs QUANTUM WELL INFRARED PHOTODETECTOR (QWIP) PALM-SIZE CAMERA

S. D. Gunapala, S. V. Bandara, J. K. Liu, E. M. Luong, M. J. McKelvey, J. M. Mumolo, C. A. Shott, N. Stetson, * and S. D. Rafol

Center for Space Microelectronics Technology, Jet Propulsion Laboratory, California Institute of Technology, Pasadena, California
* Inframetrics, Inc., 16 Esquire Road, No. Billerica, Massachusetts

ABSTRACT

A 9 μm cutoff 256x256 palm-size quantum well infrared photodetector (QWIP) camera has been demonstrated. Excellent imagery, with a noise equivalent differential temperature (NEΔT) of 23 mK has been achieved. In this paper, we discuss the development of this very sensitive long-wavelength infrared (LWIR) camera based on a GaAs/AlGaAs QWIP focal plane array (FPA) and its performance in terms of quantum efficiency, NEΔT, uniformity, and operability.

KEY WORDS: Intersubband Transition, Infrared (IR), Long-wavelength Infrared (LWIR), Focal Plane Arrays (FPAs), Gallium Arsenide (GaAs), Quantum Well Infrared Photodetectors (QWIPs), Noise Equivalent Temperature Difference (NEΔT), Infrared Imaging Cameras.

INTRODUCTION

NASA, commercial, medical, and defense applications such as Earth observation systems, astronomy, weather monitoring, thermal mapping, thermography, missile tracking, and night vision aids, etc. require high performance large format long-wavelength infrared (LWIR) detector arrays in the wavelength range of 8-16μm. Thus, NASA and Ballistic Missile Defense Organization (BMDO) have devoted a significant effort in developing highly sensitive infrared (IR) detectors and large format focal plane arrays (FPAs) based on novel "artificial" low "effective" band-gap semiconductor material systems such as GaAs/AlGaAs. Consequently, Jet Propulsion Laboratory (JPL) has started to investigate GaAs/AlGaAs based multi-quantum wells (MQWs) for IR radiation detection. Through the optimization of the detector design, light coupling schemes and development of large format FPA fabrication and packing, portable 256x256 QWIP FPA IR cameras have been realized (1,2). Similarly, a TV format (i.e., 640x486) QWIP camera which can see 8.5 μm has been demonstrated (3). These achievements bring forth great promise for myriad applications in the 6-20 μm wavelength region (4). In this paper we discuss fabrication, characterization, and performance of 256x256 LWIR QWIP FPA and the demonstration of palm-size IR camera based on this 256x256 LWIR FPA.

Improving QWIP performance depends largely on minimizing the parasitic current that plagues all light detectors, the dark current (i.e., the current that flows through a biased detector in the dark with no photons impinging on it). As we have discussed elsewhere (5), at temperatures above 45 K, the dark current of the LWIR QWIP is entirely dominated by classic thermionic emission of ground state electrons directly out of the well into the energy continuum. Minimizing this last component is critical to the commercial success of the QWIP as it allows the highly desirable high temperature FPA operation.

TEST STRUCTURE RESULTS

We have designed the bound-to-quasibound quantum well by placing the first excited state exactly at the well top as shown in Fig. 1. Each period of the MQW structure consists of a 45 Å well of GaAs (doped n = $4x10^{17}$ cm^{-3}) and a 500 Å barrier of $Al_{0.3}Ga_{0.7}As$. Fifty such periods are stacked together for higher photon absorption. Ground state electrons are provided in the detector by doping the GaAs well layers with Si. This photosensitive MQW structure is sandwiched between 0.5 μm GaAs top and bottom contact layers doped n = $4x10^{17}$ cm^{-3}, grown on a semi-insulating GaAs substrate by molecular beam epitaxy (MBE). Then a 0.7 μm thick GaAs cap layer on top of a 300 Å $Al_{0.3}Ga_{0.7}As$ stop-etch layer is grown *in situ* on top of the device structure for

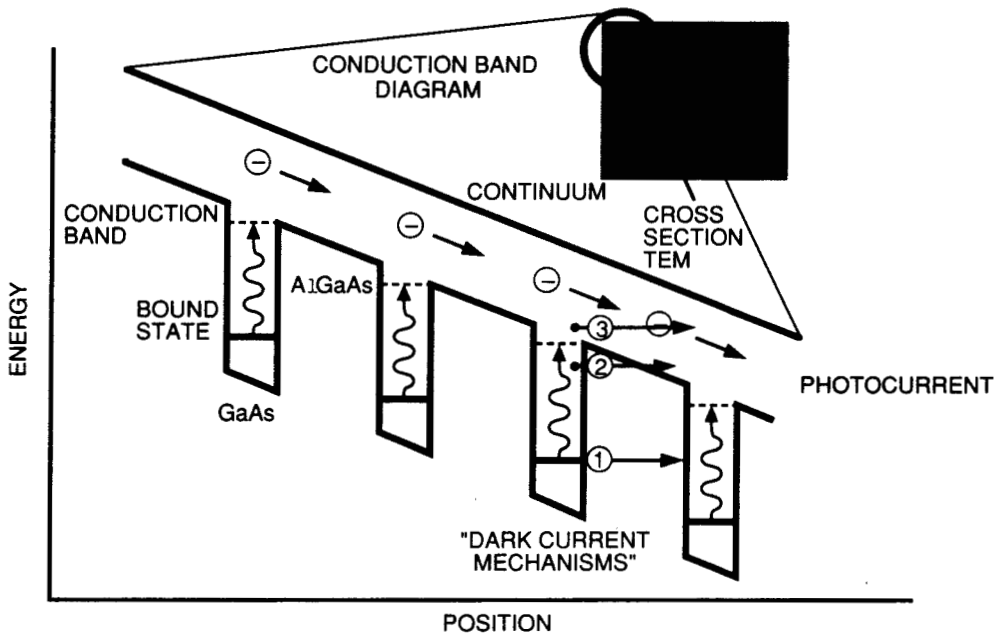

Fig. 1. Schematic diagram of the conduction band in a bound-to-quasibound QWIP in an externally applied electric field. Absorption of IR photons can photoexcite electrons from the ground state of the quantum well into the continuum causing a photocurrent. Three dark current mechanisms are also shown: (1) ground state tunneling, (2) thermally assisted tunneling, (3) and thermionic emission. The inset shows a cross-section transmission electron micrograph of a QWIP sample.

fabricate the light coupling optical cavity. The MBE grown QWIP structure is processed into 200 μm diameter mesa test structures (area = 3.14 x 10^{-4} cm^2) using wet chemical etching, and Au/Ge ohmic contacts are evaporated onto the top and bottom contact layers.

The detectors are back illuminated through a 45° polished facet (5) and a responsivity spectrum is shown in Fig. 2. The responsivity of the detector peaks at 8.4 μm and the peak responsivity (R_p) of the detector is 168 mA/W at bias V_B = -2 V. The spectral width and the cutoff wavelength are $\Delta\lambda/\lambda$= 10% and λ_c = 8.8 μm respectively. The measured absolute peak responsivity of the detector is small, from V_B = 0.0 to -0.5 V. Beyond that it increases nearly linearly with bias reaching R_P = 365 mA/W at V_B = -5 V. This type of behavior of responsivity versus bias is typical for a bound-to-quasibound QWIP. The peak quantum efficiency was 16.6% at bias V_B = -2 V for a 45° double pass. The lower quantum efficiency is due to the lower well doping density ($4x10^{17}$ cm^{-3}) as it is necessary to suppress the dark current for the highest possible operating temperature. A peak quantum efficiency as high as 25% has already been achieved with regular well doping density (i.e., $1x10^{18}$ cm^{-3}). Due to lower readout multiplexer well depth (i.e., $5x10^6$ electrons), a lower dark current is mandatory to achieve a higher operating temperature. In this case, the highest operating temperature of 74 K was determined by the cooling capacity of the small integral Sterling cooler used in an Inframetric's *InfraCAM*™ camera.

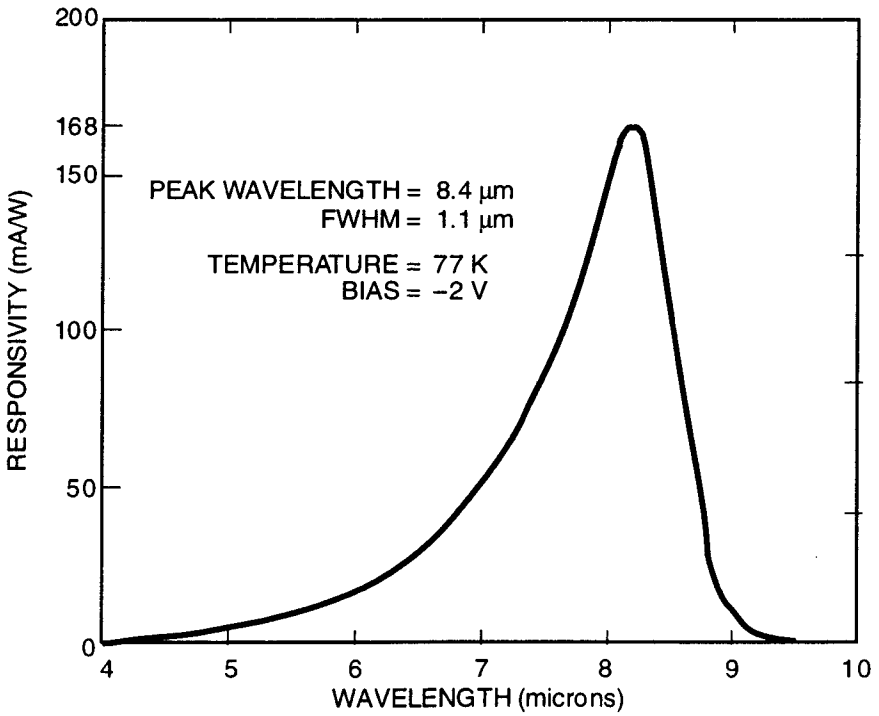

Fig. 2. Responsivity spectrum of a bound-to-quasibound LWIR QWIP test structure at temperature T = 77 K. The spectral response peak is at 8.5 μm and the long wavelength cutoff is at 8.9 μm.

The photoconductive gain g was experimentally determined using $g = i_n^2 / 4eI_D B$, where B is the measurement bandwidth, and i_n is the current noise, which was measured using a spectrum analyzer. The photoconductive gain of the detector reached 0.32 at V_B =-5 V. The peak detectivity is defined as $D_P^* = R_P\sqrt{AB}/i_n$, where R_P is the peak responsivity, A is the area of the detector and A = 3.14×10^{-4} cm^2. The measured peak detectivity at bias V_B = -2.0 V and temperature T = 70 K is 2.0×10^{11} $cm\sqrt{Hz}/W$. Figure 3 shows the bias dependence of peak detectivity at temperatures 70, 75 and 80 K. These detectors show background limited performance (BLIP) at bias V_B = -2 V and temperature T = 72 K for 300 K background with f/2 optics.

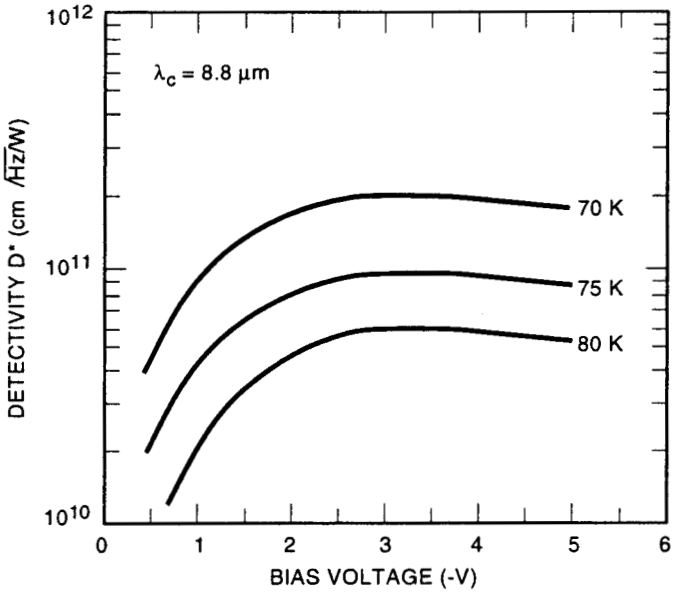

Fig. 3. Detectivity as a function of bias voltage at temperatures T = 70 and 77 K.

IMAGING ARRAYS

Although random reflectors have achieved relatively high quantum efficiencies with large test device structures, it is not possible to achieve the similar high quantum efficiencies with random reflectors on small FPA pixels due to the reduced width-to-height aspect ratios. In addition, it is difficult to fabricate random reflectors for shorter wavelength detectors relative to very long-wavelength detectors (i.e., 15 μm) due to the fact that feature sizes of random reflectors are linearly proportional to the peak wavelength of the detectors. For example, the minimum feature size of random reflectors of 15 μm cutoff and 9 μm cutoff FPAs were 1.25 and 0.6 μm respectively, and it is difficult to fabricate sub-micron features by contact photolithography. As a result, the random reflectors of the 9 μm cutoff FPA were less sharp and had fewer scattering centers compared to the random reflectors of the 15 μm cutoff QWIP FPA. It is well known that QWIPs do not absorb radiation incident normal to the surface unless the IR radiation has an electric field component normal to the layers of superlattice (growth direction) (5). As we have discussed before (5), more IR light can be coupled to the

QWIP detector structure by incorporating a two dimensional grating surface (6) on top of the detectors which also removes the light coupling limitations and makes two dimensional QWIP imaging arrays feasible. This two dimensional grating structure was fabricated on the detectors by using standard photolithography and CCl_2F_2 selective dry etching.

After the 2-D grating array (calculations of the 2-D grating parameters and light coupling experiments were extensively discussed in references 5 and 6) was defined by the photolithography and dry etching, the photoconductive QWIPs of the 256x256 FPAs were fabricated by wet chemical etching through the photosensitive $GaAs/Al_xGa_{1-x}As$ multi-quantum well layers into the 0.5 μm thick doped GaAs bottom contact layer. The pitch of the FPA is 38 μm and the actual pixel size is 28x28 μm^2. The 2-D grating reflectors on top of the detectors were then covered with Au/Ge and Au for Ohmic contact and reflection. Twenty five QWIP FPAs were processed on a 3-inch GaAs wafer. Indium bumps were then evaporated on top of the detectors for Si readout circuit (ROC) hybridization. A single QWIP FPA was chosen and hybridized (via indium bump-bonding process) to a 256x256 CMOS multiplexer (Amber AE-166) and biased at V_B = -2.0 V. At temperatures below 72 K, the signal to noise ratio of the system is limited by array non-uniformity, multiplexer readout noise, and photo current noise (for f/2 optics). At temperatures above 72 K, temporal noise due to the QWIP's higher dark current becomes the limitation. As mentioned earlier this higher dark current is due to thermionic emission and thus causes the charge storage capacitors of the readout circuitry to saturate. Since the QWIP is a high impedance device, it should yield a very high charge injection coupling efficiency into the integration capacitor of the multiplexer. In fact Bethea *et al.* (7) have demonstrated charge injection efficiencies approaching 90%. Charge injection efficiency can be obtained from (8)

$$\eta_{inj} = \frac{g_m R_{Det}}{1 + g_m R_{Det}} \left[\frac{1}{1 + \frac{j\omega C_{Deg} R_{Det}}{1 + g_m R_{Det}}} \right] \qquad (1)$$

where g_m is the transconductance of the MOSFET and it is given by $g_m = eI_{Det}/kT$. The differential resistance R_{Det} of the pixels at -2 V bias is $2.6x10^{10}$ Ohms at T=70 K and detector capacitance C_{Det} is $3.0x10^{-14}$ F. The detector dark current I_{Det} = 34 pA under the same operating conditions. According to equation (1) the charge injection efficiency η_{inj}=90% at a frame rate of 60 Hz. The FPA was back-illuminated through the flat thinned substrate membrane (thickness ≈ 1300 Å). This initial array gave excellent images with 99.87% of the pixels working (number of dead pixels ≈ 88) , demonstrating the high yield of GaAs technology. The operability was defined as the percentage of pixels having noise equivalent differential temperature less than 100 mK at 300 K.

The background temperature T_B = 300 K, the area of the pixel A = $(28\ \mu m)^2$, the f number of the optical system is 2, and the frame rate is 60 Hz. Figure 4 shows the measured NEΔT of the FPA at an operating temperature of T = 70 K, bias V_B = -2 V for 300 K background and the mean value is 23 mK. The uncorrected NEΔT nonuniformity

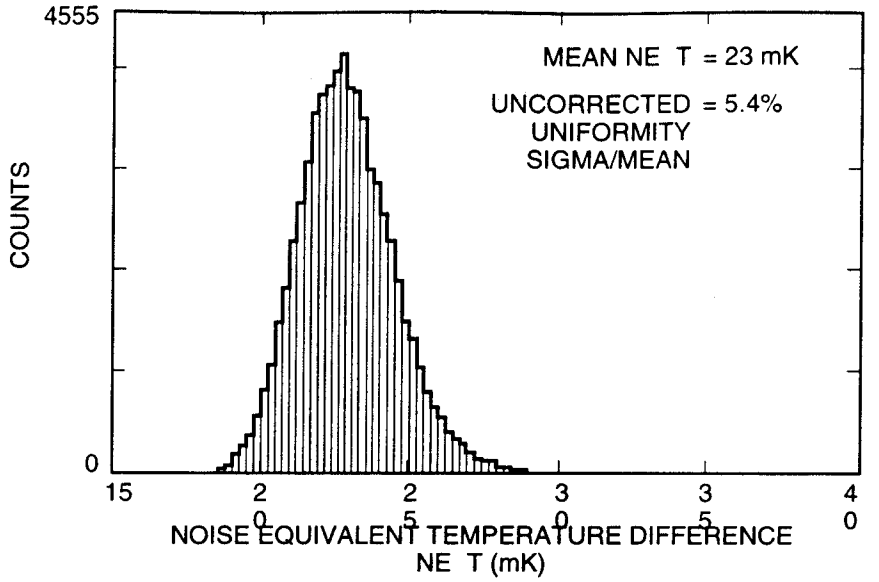

Fig. 4. Uncorrected noise equivalent differential temperature (NEΔT) histogram of the 65,536 pixels of the 256x256 array showing the uniformity of the FPA. The lowest QWIP FPA nonuniformity achieved is <2%. The uncorrected non-uniformity (= standard deviation/mean) of the FPA is only 5.4% including 1% non-uniformity of ROC and 1.4% non-uniformity due to the cold-stop not being able to give the same field of view to all the pixels in the FPA.

(sigma/mean) is 5.4%. This agrees reasonably with our estimated value of 8 mK based on test structure data. The peak quantum efficiency of the FPA was 5.7% (lower focal plane array quantum efficiency is attributed to 54% fill factor, 30% substrate reflection and 90% charge injection efficiency) and this corresponds to an average of two passes of IR radiation (equivalent to a single 45° pass) through the photosensitive MQW region. Figure 5 shows the quantum efficiency histogram of the FPA, and the uncorrected nonuniformity (sigma/mean) is 5.5%.

PALM-SIZE CAMERA

A 256x256 QWIP FPA hybrid was mounted onto a 130 mW integral Sterling closed-cycle cooler assembly and installed into an Inframetric's *InfraCAM*™ camera-body, to demonstrate a palm-size LWIR camera (shown in Fig. 6). The camera is equipped with a 50 mm focal length f/1.3 germanium lens with an 11.2 degree field of view designed to be transparent in the 8-12 μm wavelength range to be compatible with the QWIP's 8.5 μm operation. The dimensions of the camera are 5.3"x 9.7"x 2.5" and it weighs less than three pounds including battery, lens, and viewfinder. The lens assembly can easily be removed, and other lenses can be attached to provide other fields of view or higher resolution images. The power consumption of the camera is 5.5 Watts and it runs more than two hours with a 2400 mAh, 6-Volt camcorder battery.

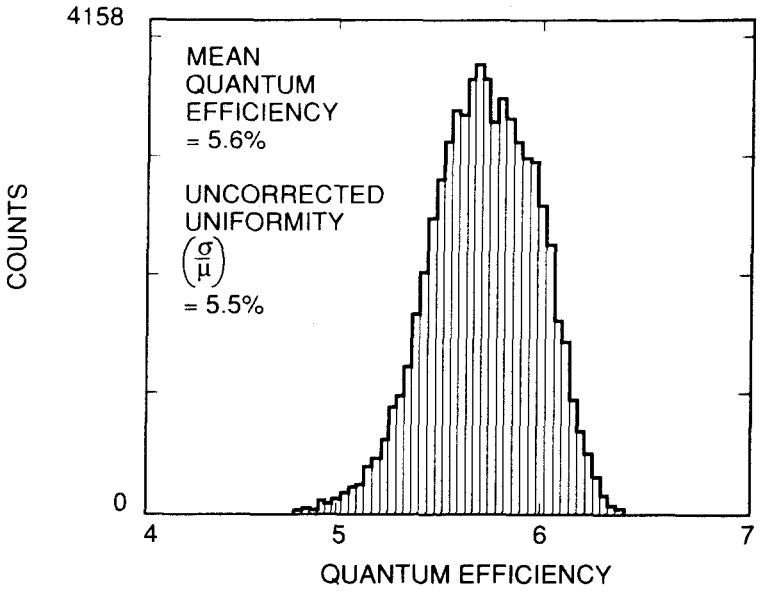

Fig. 5. Uncorrected quantum efficiency histogram of the 65,536 pixels of the 256x256 array showing a high uniformity of the FPA.

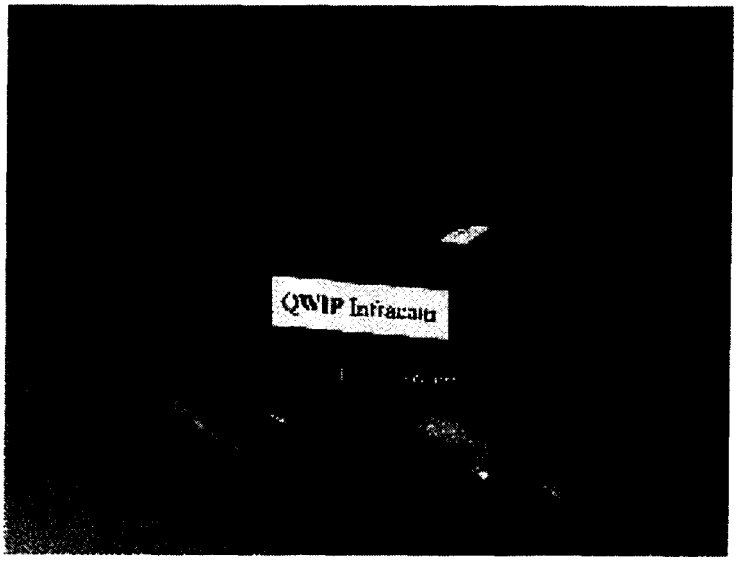

Fig. 6. Picture of 256x256 palm-size long-wavelength QWIP *InfraCAM*™.

The measured mean NEΔT of the QWIP *InfraCAM*™ is 38 mK at an operating temperature of T = 74 K and bias V_B = -2 V, for a 300 K background (the higher NEΔT is mostly due to the higher operating temperature). Figure 7 shows the DC signal histogram before two-point correction. It is worth noting that all uncorrected

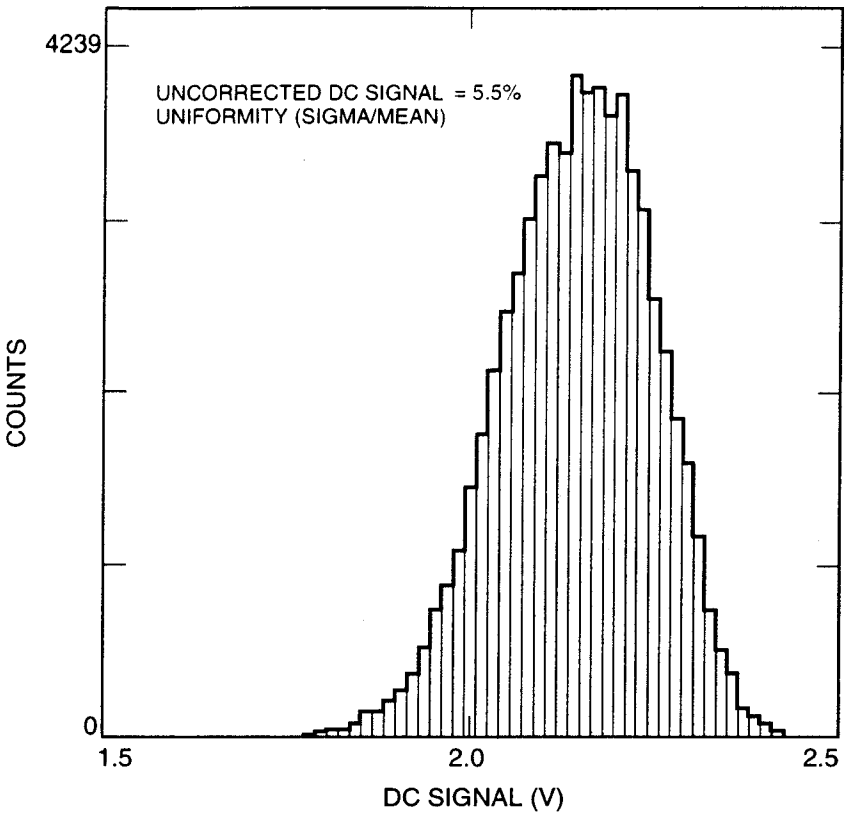

Fig. 7. Uncorrected DC signal histogram of the 65,536 pixels of the 256x256 array showing the high uniformity of the FPA.

nonuniformities (NEΔT, quantum efficiency, and DC signal) of the 65,536 pixels of the 256x256 FPA are about 5.5% (= sigma/mean). The nonuniformity after two-point (17° and 27° Celsius) correction improves to an impressive 0.03% (See Fig. 9). As mentioned earlier, this high yield is due to the excellent GaAs growth uniformity and the mature GaAs processing technology. The dead pixel scatter of the FPA is shown in Fig. 8. Pixels having NEΔT>100 mK are counted as dead pixels, thus, the operability of this FPA is 99.87%. However, the actual number of dead pixels (i.e., no photo response) is less than 10, thereby making pixel replacement software unnecessary. It is important to mention that this palm-size LWIR camera does not require any calibrations or nonuniformity corrections prior to data acquisition. Instead, it uses a nonuniformity correction table (i.e., gains and offsets) stored in its read-only-memory (ROM) for its entire life. It is worth noting that this technique is successful solely due to the higher stability (or lower 1/f noise) of QWIP FPAs. In other words, the nonuniformities of QWIP FPAs are almost entirely independent of time.

The minimum resolvable temperature difference was measured by two observers. While the collection of the data does not adhere to the generally accepted requirements of having multiple observers, the data is consistent with the NEΔT measurement and worth reporting. Data was taken with four-bar targets ranging in spatial frequency from 0.1 cycles/milli radian up to 0.9 cy/mr, the first target where no contrast could be measured (unclear). At the lowest spatial frequency, the MRDT was 10 mK (or 10 mCelsius). Figure 10 shows MRTD plotted as a function of the spatial frequency cy/mr.

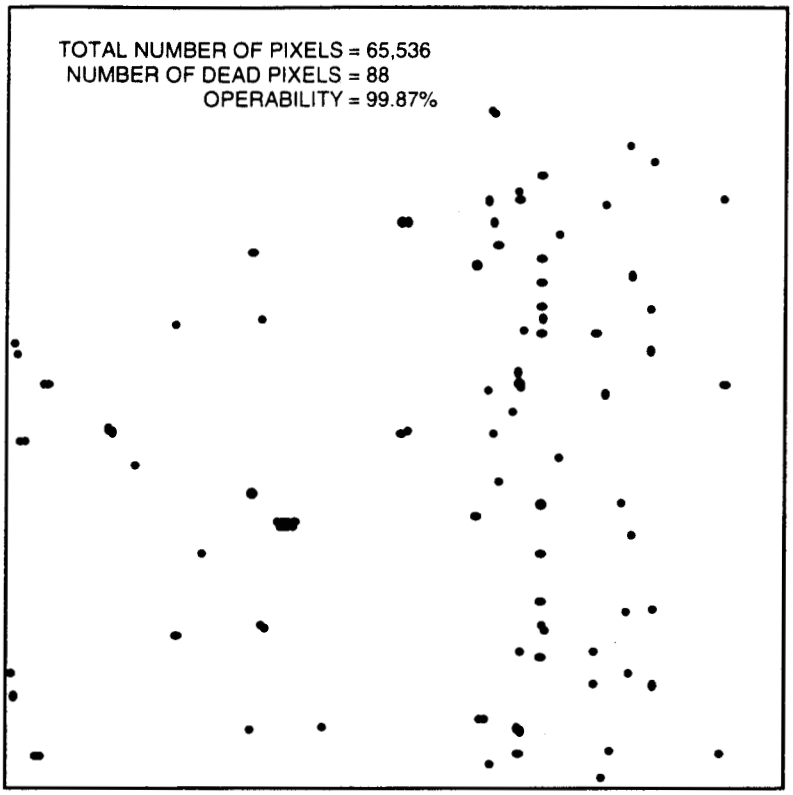

Fig. 8. Dead pixel scatter. Pixels having NEΔT>100 mK are counted as dead pixels. Thus, the operability of this FPA is 99.87%. However, the actual number of dead pixels (i.e., no photo response) is less than 10.

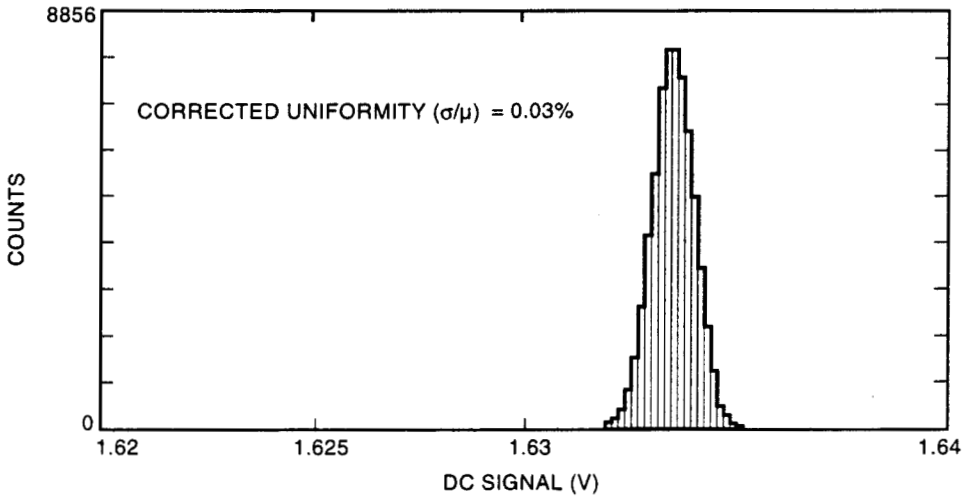

Fig. 9. Residual DC signal histogram of the 65,536 pixels of the 256x256 after two point correction. The corrected non-uniformity (= standard deviation/mean) of the FPA is only 0.03%.

Video images were taken at a frame rate of 60 Hz at temperatures as high as T = 74 K using a ROC capacitor having a charge capacity of $8x10^6$ electrons (the maximum number of photoelectrons and dark electrons that can be counted in the time taken to read

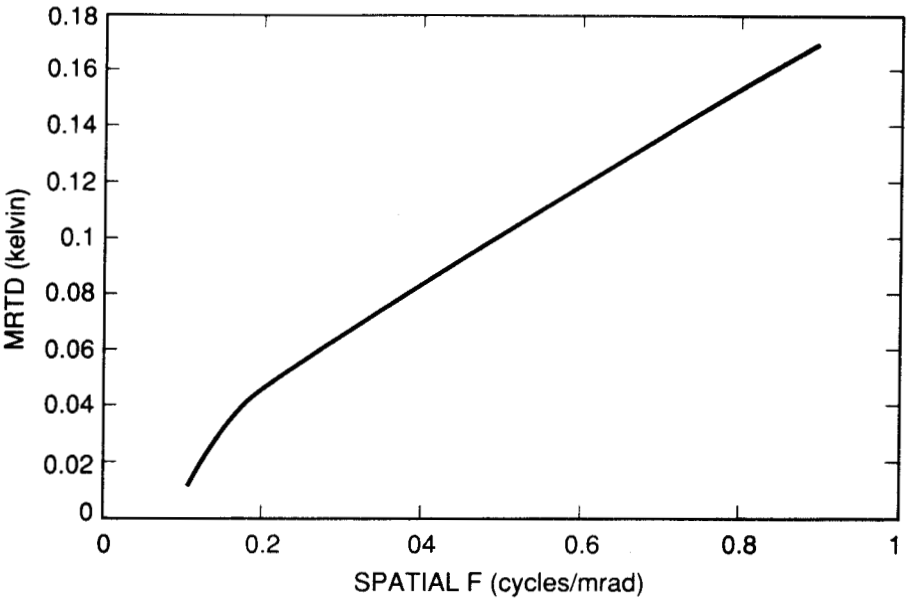

Fig. 10. Minimum resolvable temperature difference (MRTD) plotted as a function of the spatial frequency.

each detector pixel). Figure 11 shows one frame of a video image taken with a 9 μm cutoff 256x256 QWIP camera. This image demonstrate the high sensitivity of the 256x256 QWIP *InfraCAM*™.

Fig. 11. One frame of video image taken with the 9 μm cutoff 256x256 QWIP *InfraCAM*™.

It should be noted that this particular FPA is far from optimum and it does not represent the best nonuniformity and operability. The lowest uncorrected nonuniformities achieved in QWIP FPAs are 2% and the highest operabilities are >99.9%. The gratings were not optimized (as described earlier) for maximum light coupling efficiency and the

multiplexer used was a photovoltaic InSb multiplexer which is not optimized to supply the proper bias and impedance levels required by photoconductive QWIPs. Implementation of these improvements should significantly enhance the QWIP FPA operating temperature (i.e., 80 K for 9 μm).

ACKNOWLEDGMENTS

The research described in this paper was performed by the Center for Space Microelectronics Technology, Jet Propulsion Laboratory, California Institute of Technology, and was jointly sponsored by the BMDO/Innovative Science and Technology Office, and the NASA Office of Space Science.

REFERENCES

1. D. Gunapala, J. K. Liu, J. S. Park, M. Sundaram, C. A. Shott, T. Hoelter, T. L. Lin, S. T. Massie, P. D. Maker, R. E. Muller, and G. Sarusi, IEEE Trans. Electron Devices 44, 51 (1997).

2. R. Breiter, W. Cabanski, R. Koch, W. Rode, and J. Ziegler, SPIE 3379, 423 (1998).

3. D. Gunapala, S. V. Bandara, J. K. Liu, W. Hong, M. Sundaram, P. D. Maker, R. E. Muller, C. A. Shott, and R. Carralejo, IEEE Trans. Electron Devices 45, 1890 (1998).

4. S. D. Gunapala, S. V. Bandara, J. K. Liu, W. Hong, E. M. Luong, J. M. Mumolo, M. J. McKelvey, D. K. Sengupta, A. Singh, C. A. Shott, R. Carralejo, P. D. Maker, J. J. Bock, M. E. Ressler, M. W. Werner, and T. N. Krabach, SPIE 3379, 382 (1998).

5. S. D. Gunapala and K. M. S. V. Bandara, Physics of Thin Films, Academic Press, 21, 113 (1995).

6. J. Y. Andersson, L. Lundqvist, and Z. F. Paska, Appl. Phys. Lett. 58, 2264 (1991).

7. C. G. Bethea, B. F. Levine, M. T. Asom, R. E. Leibenguth, J. W. Stayt, K. G. Glogovsky, R. A. Morgan, J. D. Blackwell, and W. J. Parrish, "Long Wavelength Infrared 128 x 128 AlxGa1-xAs/GaAs Quantum Well Infrared Camera and Imaging System," *IEEE Trans. Electron. Devices*, vol. 40, pp. 1957-1963, 1993.

8. L. J. Kozlowski, G. M. Williams, G. J. Sullivan, C. W. Farley, R. J. Andersson, J. Chen, D. T. Cheung, W. E. Tennant, and R. E. DeWames, "LWIR 128x128 GaAs/AlGaAs Multiple Quantum Well Hybrid Focal Plane Array," *IEEE Trans. Electron. Devices* , vol. ED-38, pp. 1124-1130, 1991.